Electronic Supplementary Information (ESI) for

Phase-dependent Friction of Nanoconfined Water Meniscus

Xin Zhao, Hu Qiu*, Wanqi Zhou, Yufeng Guo and Wanlin Guo

State Key Laboratory of Mechanics and Control of Mechanical Structures and Key Laboratory for Intelligent Nano Materials and Devices of MOE, Institute of Nano Science, Nanjing University of Aeronautics and Astronautics, Nanjing, 210016, China.

*Email: qiuhu@nuaa.edu.cn

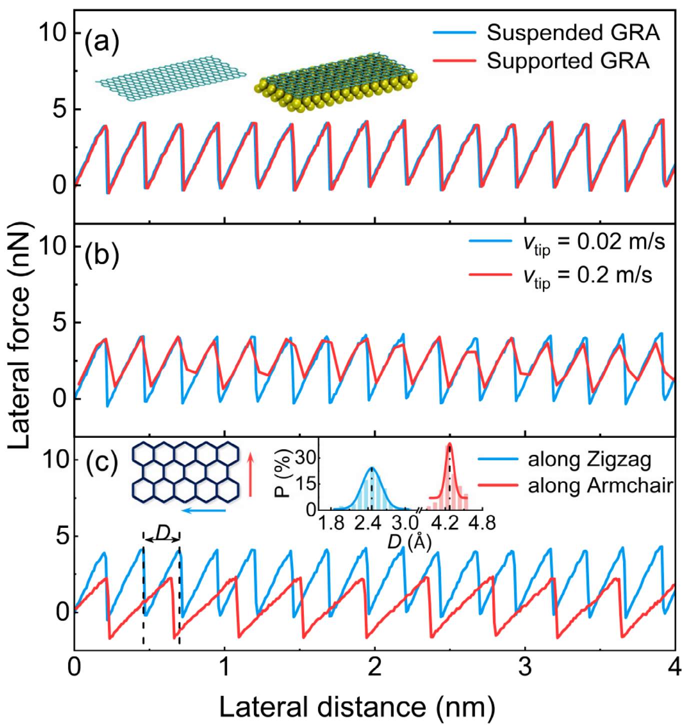

Fig. S1 Impact of key simulation conditions on the friction of water meniscus (1I-2I-3I). (a) Lateral force traces for the water meniscus on graphene with (denoted as "supported GRA") and without (denoted as "suspended GRA") an underneath gold substrate. (b) Lateral force traces for the water meniscus at tip sliding velocities v_{tip} = 0.02 and 0.2 m/s. (c) Lateral force traces for the water meniscus when the tip is sliding along the armchair and zigzag direction of the graphene layer. The right inset shows the probability distribution of the stick-slip period, *D*, with solid lines being Gaussian fits.

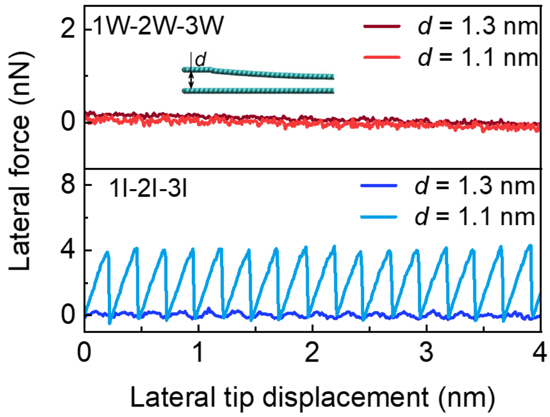

Fig. S2 Friction curves at different phase states when increasing the largest tip-substrate separation *d* from 1.1 nm (used in the main text) to 1.3 nm.

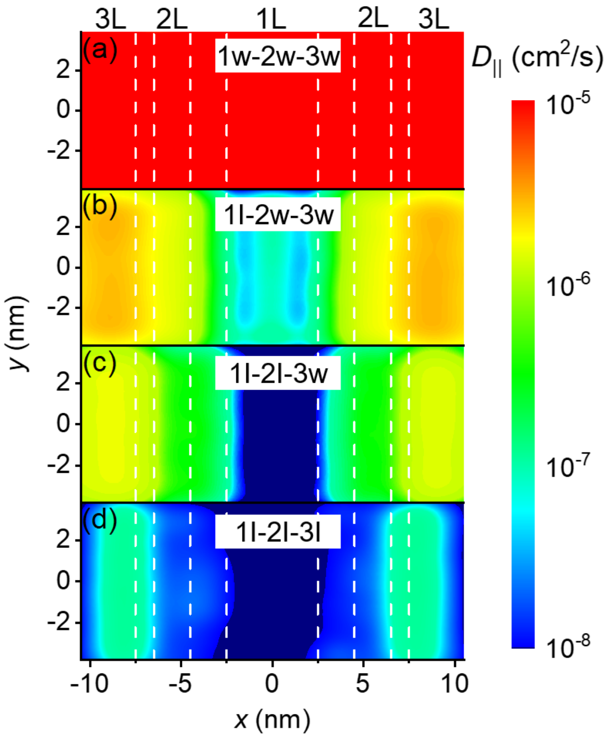

Fig. S3 Contour plots of lateral diffusion coefficient $D_{||}$ of water in the meniscus at different phase states.

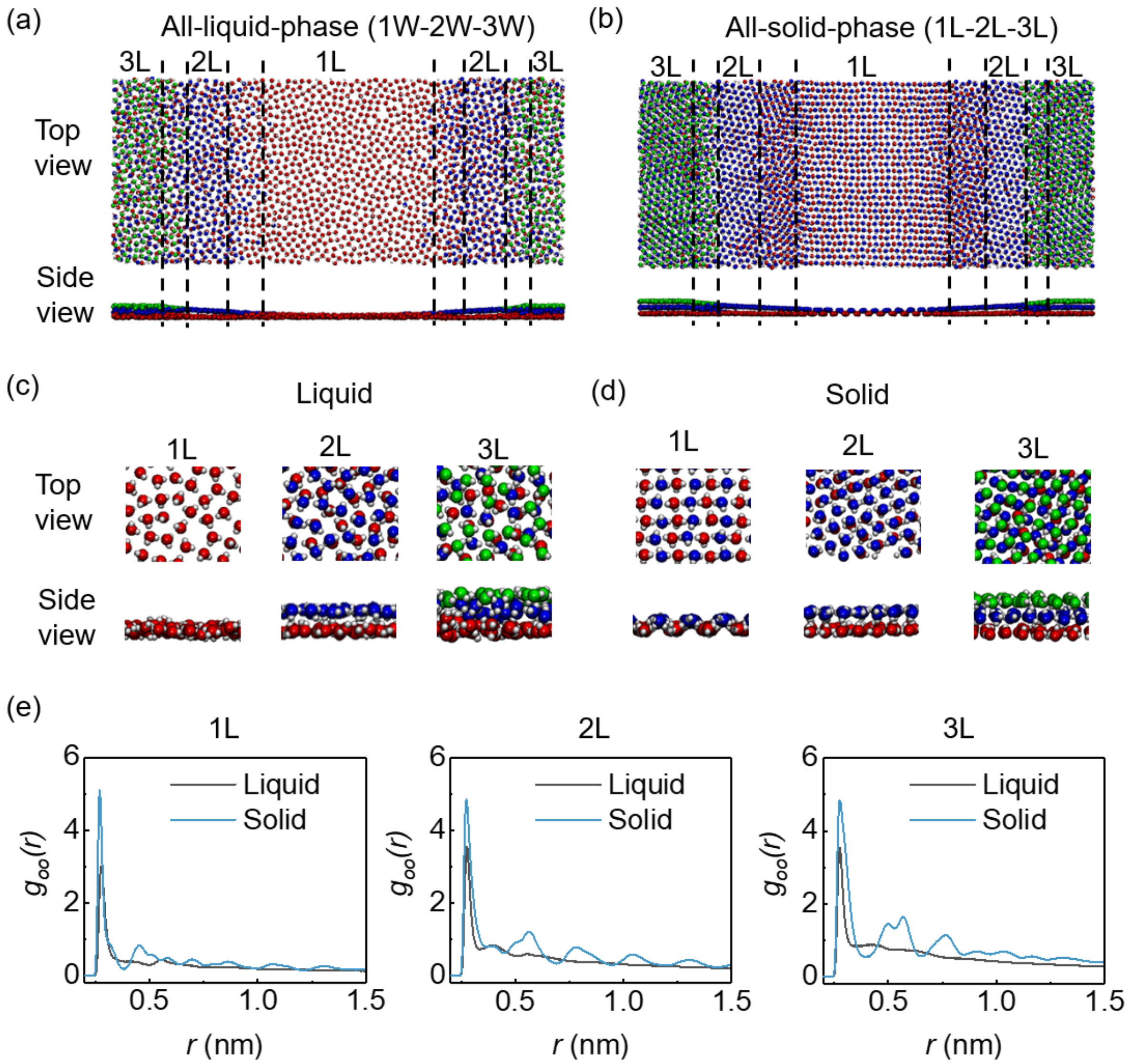

Fig. S4 Structures of the meniscus. (a,b) Snapshots showing the configurations of the meniscus at the all-liquid-phase (a) and all-solid-phase (b) states. (c,d) Magnified views of water structures in the 1L, 2L and 3L domains at the two phase states. Green, blue, and red spheres represent water oxygen atoms in the top, middle, and bottom planes, and grey spheres are hydrogen atoms. (e) Oxygen-oxygen radial distribution function $g_{OO}(r)$ of water in different domains at liquid and solid states.

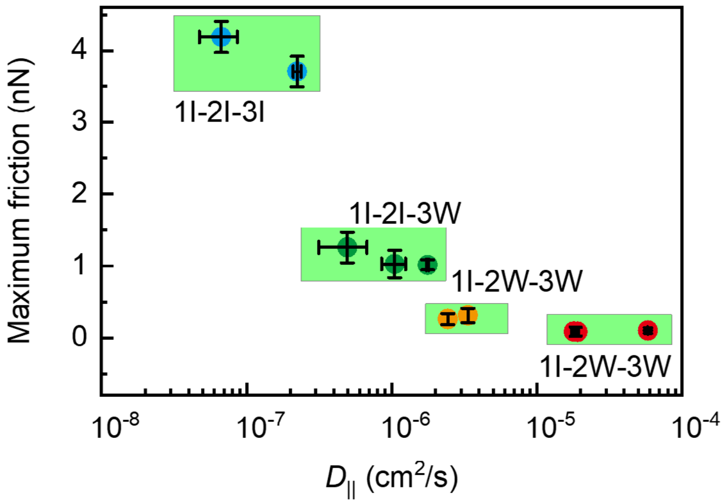

Fig. S5 Variation of maximum friction forces with average lateral diffusion coefficient $D_{||}$. The error bars indicate the standard deviation of friction obtained from three independent simulation runs. Note that the error bars of some data points are too small to be visible.

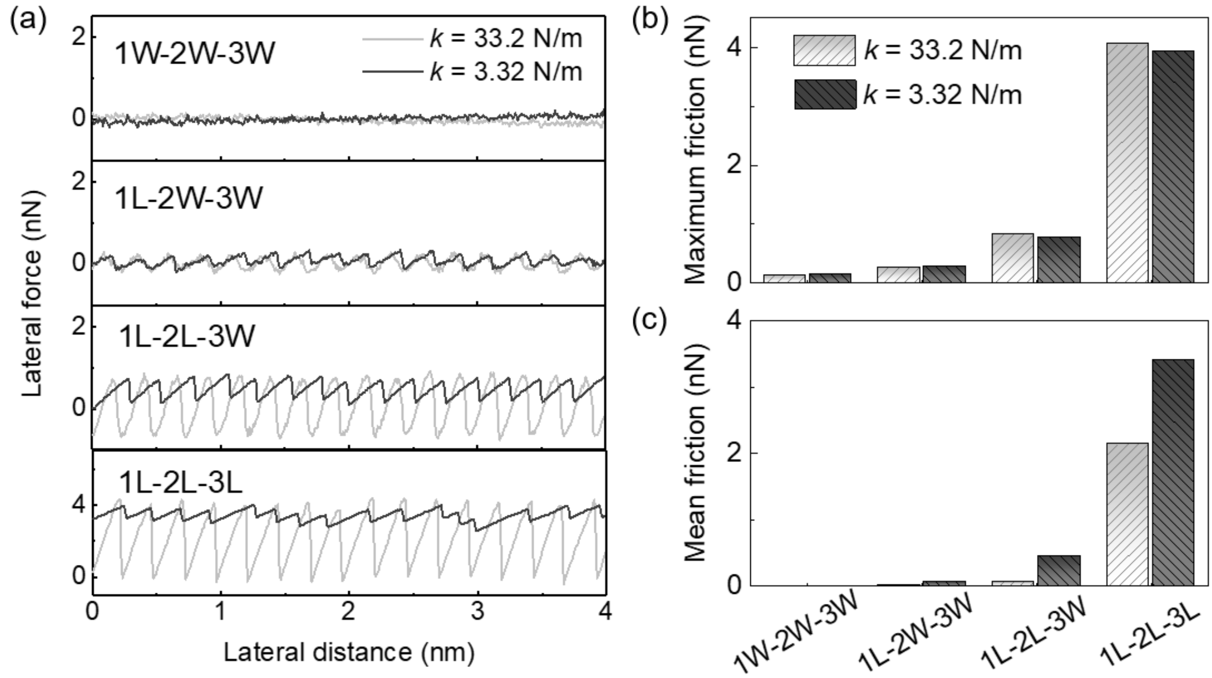

Fig. S6 Impact of the spring stiffness *k* attached to the tip on measured friction. (a) Comparison of lateral force traces measured with *k* = 33.2 N/m (used in most simulations) between 3.32 N/m at four typical phase states of the meniscus. (b,c) Comparison of maximum (b) and mean (c) friction forces obtained with different *k*.

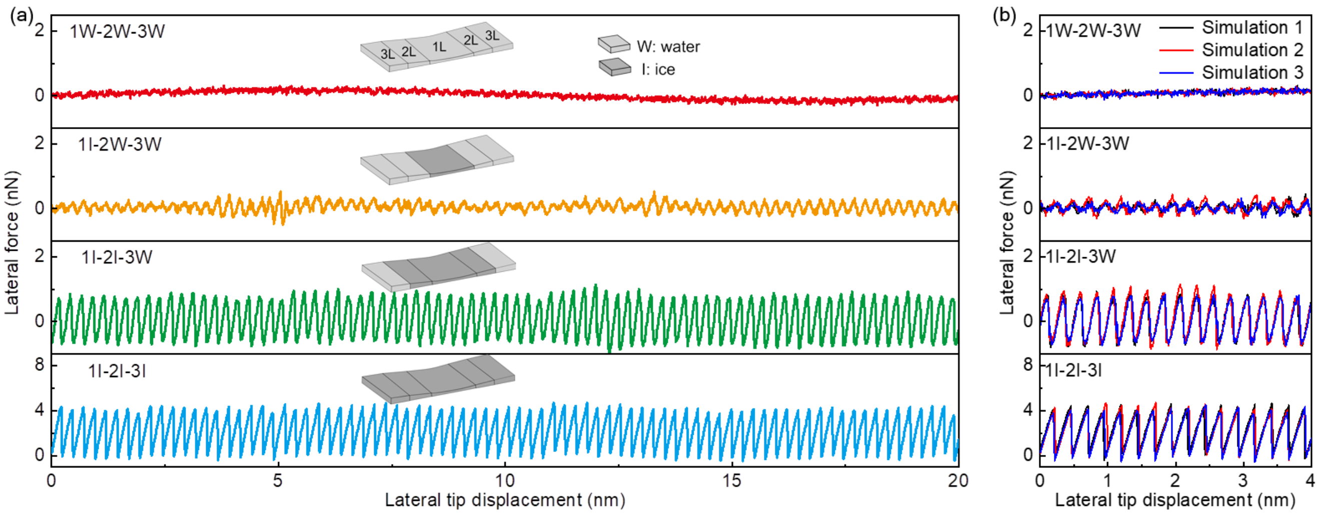

Fig. S7 (a) Lateral force traces in very long simulations (1000 ns) for the water meniscus at four typical phase states. These curves are supplemental to those in Fig. 2b in the main text. (b) Lateral force traces in repeated simulation runs at four typical phase states. At a given state, the repeated runs were performed for a same initial configuration but with different assignment of initial velocities of water molecules.

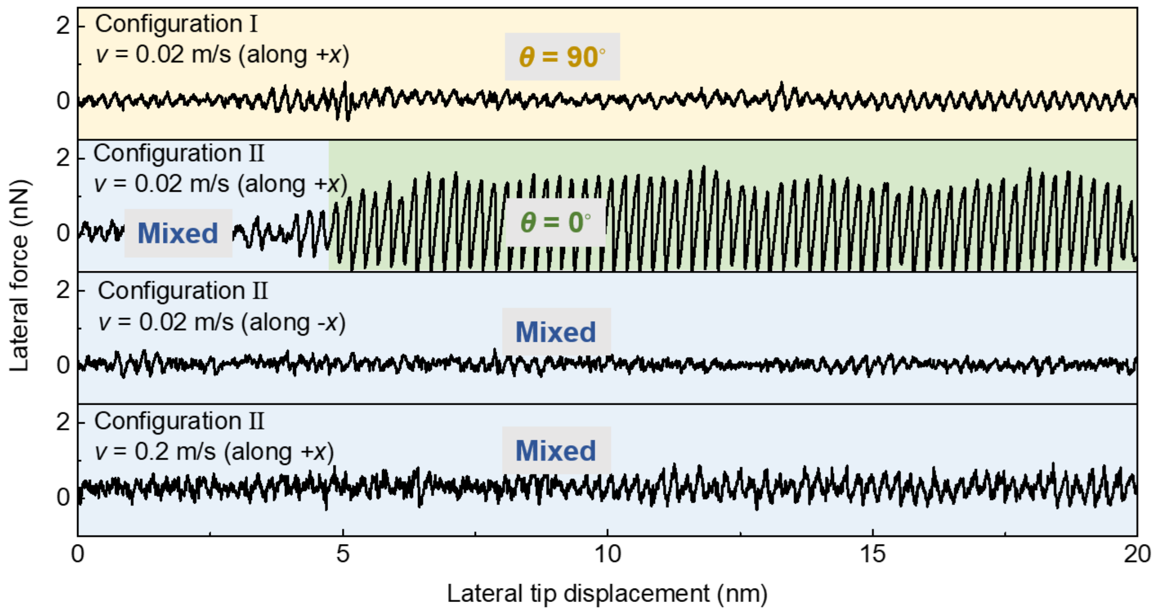

Fig. S8 Raw data of lateral force traces used to determine overall probabilities of different phase orientations at the 1I-2W-3W state. The initial configuration I (ϑ = 90°) was obtained by an increase of the lateral pressure from 0.1 MPa to 300 MPa in a 4 ns simulation, followed a decrease to 200 MPa in another 4 ns simulation, while the initial configuration II ("mixed") was obtained by directly increasing the pressure from 0.1 MPa to 200 MPa in a 4 ns simulation. Different sliding velocities v or directions (along the $+x$ or $-x$ direction) were considered for friction measurement based on configuration II.

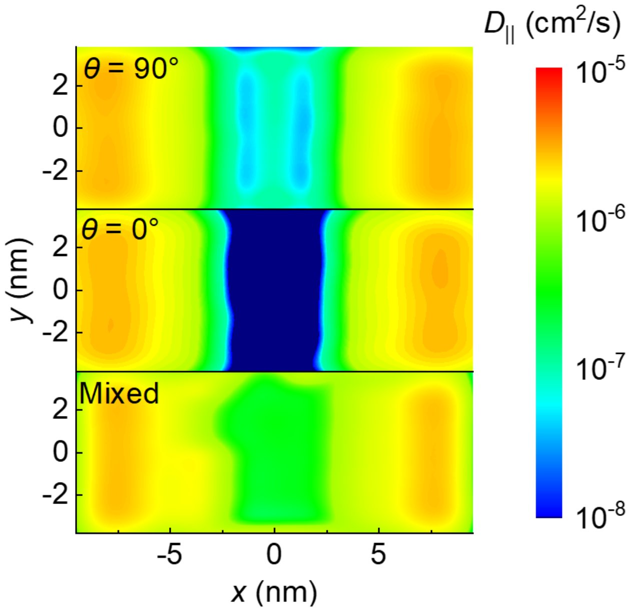

Fig. S9 Contour plot of lateral diffusion coefficient $D_{||}$ of the water meniscus (1I-2W-3W) containing 1L ice domain with different row orientation angles ϑ.

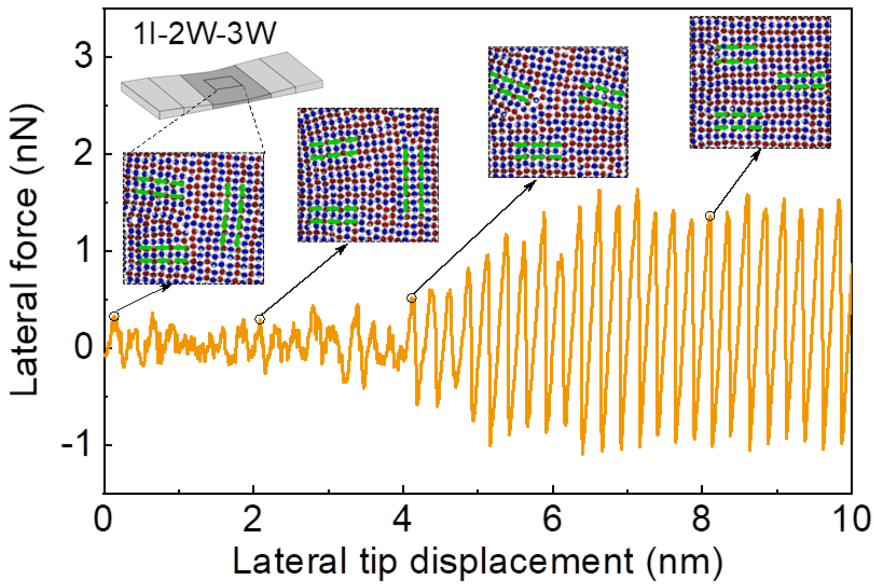

Fig. S10 Lateral force trace showing the spontaneous transition of the central 1L ice domain from a "mixed" phase into a uniformly orientated phase (ϑ = 0°). The insets show typical simulation snapshots illustrating the transition.

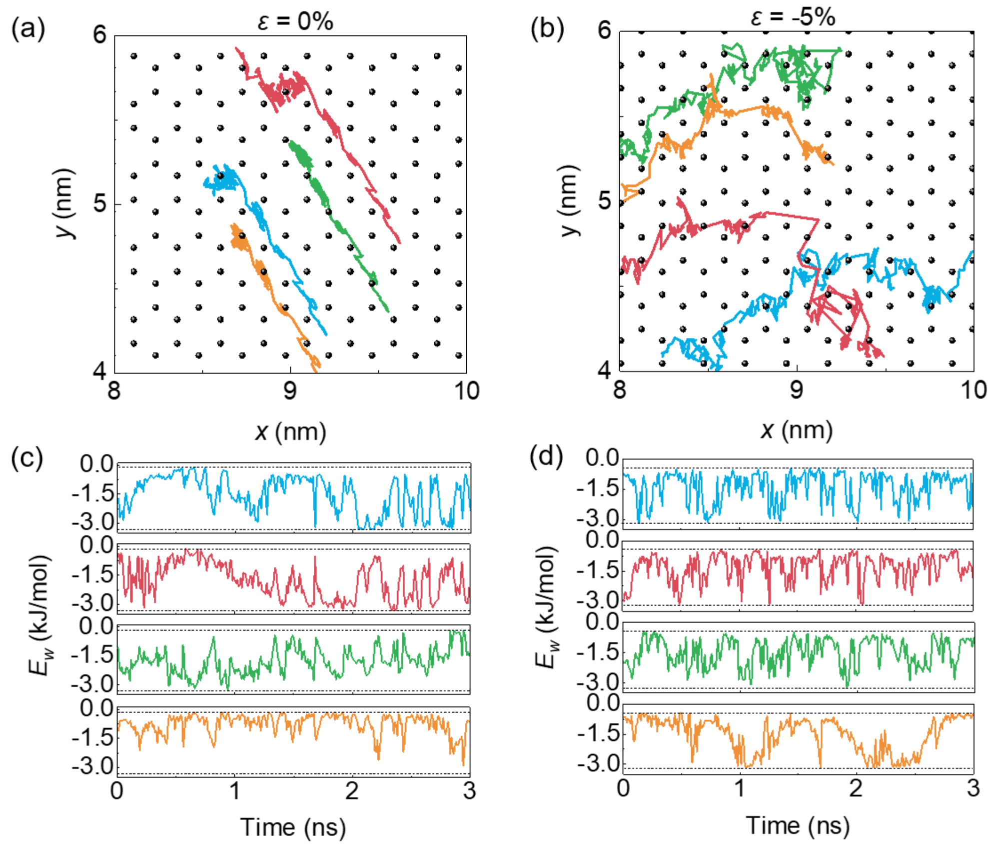

Fig. S11 In-plane trajectories of several randomly selected water molecules (a,b) and corresponding energy profiles (c,d) in a 3 ns time period on graphene subjected to strains at ε = 0% (a,c) and -5% (b,d). The horizontal dashed lines indicate the maximum and minimum of the ideal energy landscapes shown in Fig. 4d and 4e.